Supplemental material for "Mori generalized master equations offer an efficient route to predict and interpret polaron transport"

Srijan Bhattacharyya,[1] Thomas Sayer,[1] and Andrés Montoya-Castillo[1, a)]

Department of Chemistry, University of Colorado Boulder, Boulder, CO 80309, USA

[a)] Andres.MontoyaCastillo@colorado.edu

I. DISPERSIVE HOLSTEIN MODEL

The dispersive Holstein Hamiltonian can be written as

$$\hat{H} = \sum_{i}^{N} \left(\epsilon_i + \hat{V}_{B,i}\right)\hat{a}_i^\dagger \hat{a}_i + \sum_{\langle ij \rangle}^{N} v_{ij}\hat{a}_i^\dagger \hat{a}_j + \sum_{i}^{N} \hat{H}_{B,i}, \tag{S1}$$

$$\hat{H}_{B,i} = \frac{1}{2}\sum_{\alpha}\left[\hat{P}_{i,\alpha}^2 + \omega_{i\alpha}^2 \hat{X}_{i,\alpha}^2\right], \tag{S2}$$

$$\hat{V}_{B,i} = \sum_{\alpha} c_{i,\alpha}\hat{X}_{i,\alpha}, \tag{S3}$$

where the fermions (electrons or holes whose creation and annihilation operators are $\hat{a}_i^\dagger$ and $\hat{a}_j$) are assumed to be described by a tight binding system Hamiltonian parameterized by site energies ϵ_i and hopping integrals v_{ij}. Local nuclear motions are assumed to cause Gaussian fluctuations of the site energies, enabling one to write the local nuclear environment as a set of harmonic modes localized on site i with momenta $\hat{P}_\alpha$, positions $\hat{X}_\alpha$, and frequencies ω_α. The coupling between the fermions and bosons associated with a given site is linear in the bosonic coordinates, with the coupling constants $c_{i,\alpha}$ given by the site's spectral density

$$\xi_i(\omega) = \frac{\pi}{2}\sum_{\alpha}\frac{c_{i,\alpha}^2}{\omega_{i\alpha}}\delta(\omega - \omega_{i\alpha}). \tag{S4}$$

The $\xi_i(\omega)$ for each site are assumed to be equivalent and take the Debye form commonly used to capture the dissipation in the condensed phase

$$\xi(\omega) = \frac{\eta\omega_c\omega}{\omega^2 + \omega_c^2}. \tag{S5}$$

Here, $\eta/2$ is the reorganization energy and $1/\omega_c$ is the timescale at which the phonon environment decorrelates. Since we focus on a purely homogeneous lattice, all parameters become site-independent, with $\epsilon_i = 0$. Different instances of the model are thus uniquely defined by the set $[\eta, \omega_c, v, \beta]$ which we dimensionalize to $[\eta/v, \omega_c/v]$ with β fixed at 300 K throughout. We employ cyclical boundary conditions since our previous work[S1] demonstrated that non-periodic models do not exhibit a well-defined DC mobility, except in the limit of an infinitely large system.

II. MORI GQME

To derive a GQME for the current autocorrelation function directly, we employ a Mori-type projector

$$\mathcal{P} = |\hat{J})(\hat{J}|\hat{J})^{-1}(\hat{J}|. \tag{S6}$$

In contrast to previous uses of the Mori projector for quantum equilibrium time correlation functions[S2–S4] we define the inner product to yield the direct correlation function rather than the Kubo-transformed counterpart,

$$(A|\hat{\mathcal{O}}|A) = \frac{1}{Z}\mathrm{Tr}[e^{-\beta H}A^{\dagger}\hat{\mathcal{O}}A], \tag{S7}$$

where $\hat{\mathcal{O}}$ is a superoperator, like the Liouvillian, $\mathcal{L} \equiv [H, \dots]$. This projector satisfies the conditions for its validity: idempotency $\mathcal{P}^2 = \mathcal{P}$ and orthogonality $\mathcal{PQ} = 0$, where $\mathcal{Q} = \mathbb{1} - \mathcal{P}$ is the complementary projector. Traditionally, one adopts the Kubo-transformed correlation function because of the natural orthogonality of the cross-correlation function of the dynamical variable in the projector, $\hat{J}$ in this case, and its derivative. When we augment the projector with the derivative of the current in Section IV, we diagonalize the correlation matrix directly to ensure the idempotency of the projector.

This definition for the projector enables us to construct the current autocorrelation function, $C_{JJ}(t)$, as follows:

$$\mathcal{C}(t) = (\hat{J}|\mathrm{e}^{\mathrm{i}\mathcal{L}t}|\hat{J}) = \frac{1}{Z}\mathrm{Tr}[e^{-\beta H}\hat{J}\mathrm{e}^{\mathrm{i}\mathcal{L}t}\hat{J}]. \tag{S8}$$

We can immediately write down the GQME for this correlation function (for a detailed derivation of the GQME using this notation, see Refs. S5–S7),

$$\dot{\mathcal{C}}(t) = \dot{\mathcal{C}}(0)\mathcal{C}(t) - \int_0^t \mathrm{d}s\, \mathcal{K}(s)\mathcal{C}(t-s) \tag{S9}$$

where the memory kernel takes the form

$$\mathcal{K}(t) = \frac{1}{Z}\mathrm{Tr}\left[\mathrm{e}^{-\beta H}\hat{J}\mathcal{L}\mathcal{Q}\mathrm{e}^{\mathrm{i}\mathcal{Q}\mathcal{L}t}\mathcal{Q}\mathcal{L}\hat{J}\right], \tag{S10}$$

where occurrence of complementary projector in the propagator, $\mathrm{e}^{\mathrm{i}\mathcal{Q}\mathcal{L}t}$, makes it difficult to obtain. To circumvent this difficulty, we adopt the self-consistent expansion of the memory kernel[S5–S9] into auxiliary kernels $\mathcal{K}^1$ and $\mathcal{K}^3$:[S5]

$$\mathcal{K}(t) = \mathcal{K}^1(t) + \int_0^t d\tau\, \mathcal{K}^3(t-\tau)\mathcal{K}(\tau). \tag{S11}$$

One can straightforwardly construct the auxiliary kernels using the derivatives of the correlation matrix $\mathcal{C}(t)$,[S5–S7]

$$\mathcal{K}^1(t) = \ddot{\mathcal{C}}(t) - \{\dot{\mathcal{C}}(0), \dot{\mathcal{C}}(t)\} + \dot{\mathcal{C}}(0)\mathcal{C}(t)\dot{\mathcal{C}}(0), \tag{S12}$$

and

$$\mathcal{K}^3(t) = \dot{\mathcal{C}}(0)\mathcal{C}(t) - \dot{\mathcal{C}}(t), \tag{S13}$$

where $\{\hat{A}, \hat{B}\}$ corresponds to the anticommutator relation between $\hat{A}$ and $\hat{B}$. Thus, computing numerical derivatives $\dot{\mathcal{C}}(t)$ and $\ddot{\mathcal{C}}(t)$, we construct the auxiliary memory kernels. From the auxiliary kernels, one can construct the memory kernel $\mathcal{K}(t)$ using the algorithm presented in Appendix B of Ref. S10 based on the discrete reformulation of the convolution integral in the self-consistent expansion of the memory kernel, Eq. S11. To obtain the current autocorrelation function from knowledge of the memory kernel, we integrate the GQME in Eq. S9 employing a Heun integrator.[S11] To satisfy the idempotency requirement of the projector, we always employ normalized correlation function for GQME calculation i.e. $\mathcal{C}(t) = C_{JJ}(t)/C_{JJ}(0)$ for quantum correlation function and $\mathcal{C}(t) = C_{JJ}^{\mathrm{Kubo}}(0)/C_{JJ}^{\mathrm{Kubo}}(0)$ for the Kubo-transformed version.

III. HEOM DETAILS

We employ HEOM to obtain the numerically exact dynamics of the dispersive Holstein model in the first excitation subspace, corresponding to the dilute limit of one electron or hole on the lattice. HEOM integrates the bosonic variables and predicts the reduced density matrix,

$$\mathcal{C}_{kl;ij}(t) = \mathrm{Tr}\left[\rho_{k,l}(0)\mathrm{e}^{\mathrm{i}\mathcal{L}t}\hat{a}_i^\dagger\hat{a}_j\right], \tag{S14}$$

subject to any spectroscopic (nonequilibrium) initial condition, $\rho_{k,l}(0) = \hat{a}_k^\dagger\hat{a}_l e^{-\beta\hat{H}_b}/Z_b$, where $Z_b = \mathrm{Tr}[e^{-\beta\hat{H}_b}]$ is the partition function of the isolated bath.

By noting that the nonequilibrium approach to predicting the transport coefficient only requires the MSD of the polaron, $\mu = \frac{1}{2\mathrm{k_B}T}\lim_{t\to\infty}\frac{d\mathrm{MSD(t)}}{dt}$, it suffices to project onto the time-dependent site populations.[S12–S14] Thus, one needs to perform $\mathcal{O}(N)$ calculations corresponding to cases where $i = j$ and $k = l$ in Eq. S14. Because our system is fully symmetric, all such population-based starting positions are equivalent, meaning that one only needs to perform one simulation, but this simplification is not generally applicable. Indeed for a disordered system with varying site energies and hopping integrals, all positions are unique. A detailed investigation of the effects of static disorder will form the basis of future work.

To construct the population-based GQMEs in the main text we employ two distinct types of initial condition: Franck-Condon and Marcus-type. HEOM calculations, as described by Eq. S14, directly access Franck-Condon initial conditions. The Marcus initial condition corresponds to a change in the definition of $\mathrm{e}^{-\beta\hat{H}_B} \to \mathrm{e}^{-\beta\hat{H}_B^{(j)}}$, where the superscript denotes that the local bath Hamiltonian for the j^{th} site is equilibrated with its excited state, $\hat{H}_B^{(j)} =$

$\hat{H}_B + V_{B,j}$. To generate this initial condition a pre-equilibration run with all hopping integrals set to zero before a second simulation with finite hopping integrals, as outlined in Refs. S1 and S14.

Our methodology for computing equilibrium correlation functions using HEOM follows the protocol outlined in Refs. S1 and S15. It consists of a pre-equilibration step that generates the canonical initial condition $e^{-\beta\hat{H}}/Z$, followed by right-side multiplication by the current operator, $\hat{J}$, followed by real time evolution. We ensured that our pre-equilibration step was successful by varying the time of the pre-equilibration and ensuring that the resulting correlation functions converged as a function of this parameter. By examining the error between the autocorrelation functions obtained with different initialization times and the selected best one, we determine that approximately 725 fs of simulation time are required for the initial canonical density preparation. This analysis is depicted in Fig. S1. For our production runs, we used a pre-equilibration time of 4000 fs, which exceeded the minimum required pre-equilibration time in our tests.

We converged all HEOM calculations with respect to the hierarchical depth L, number of Matsubara frequencies K, and timestep δt. For example, we set $L = 22$, $K = 1$, and $\delta t = 0.25$ fs for Fig. 2. To estimate the computational resource requirements (time and memory) in Table. 1., we used the same settings. To compare results across parameter regimes, we employed $L = 26$, $K = 2$, and $\delta t = 0.1$ fs, which was sufficient to converge the most difficult parameter regime: $[\eta/v, \omega_c/v] = [400/50, 150/50]$. We also employed dynamic filtering parameters in our simulations, setting $\delta = 10^{-7}$ atomic units for the nonequilibrium simulations and canonical density preparation. For the second real time propagation in the calculation of equilibrium correlation functions, we set $\delta = 10^{-10}$ atomic units.

To construct the Kubo-transformed correlation function $C_{JJ}^{\mathrm{Kubo}}(t)$ from $C_{JJ}(t)$, we leverage their connection in the frequency domain: $C_{JJ}^{\mathrm{Kubo}}(\omega) = \frac{1-e^{-\beta\omega}}{\beta\omega} C_{JJ}(\omega)$. The factor $e^{-\beta\omega}$ behaves well for $\omega > 0$ but diverges for $\omega < 0$, complicating its use in this second region. However, since $C_{JJ}^{\mathrm{Kubo}}(\omega) = C_{JJ}^{\mathrm{Kubo}}(-\omega)$, we mirror this function around $\omega = 0$, taking the $\omega \geq 0$ region as the generator of the $\omega \leq 0$ part. Without imposing this symmetry, the inverse transform of $C_{JJ}^{\mathrm{Kubo}}(\omega)$ to $C_{JJ}^{\mathrm{Kubo}}(t)$ is prone to numerical artifacts. We generate all instances of $C_{JJ}^{\mathrm{Kubo}}(t)$ using this approach.

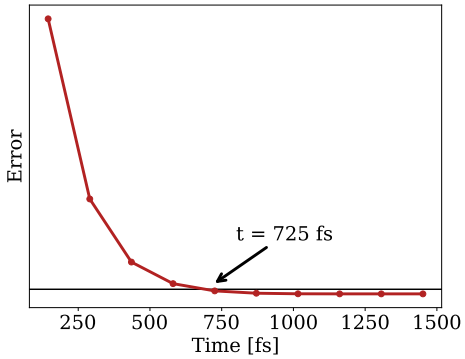

FIG. S1. Error ($||\mathrm{L}||_2$ norm of the difference) between the current autocorrelation function computed with different equilibration times and 4000 fs equilibration time. The cut-off for error is chosen as 10^{-7} (black solid line) leading to 725 fs as sufficient for preparing the initial condition for the equilibrium autocorrelation function. $\eta/v = 6.46, \omega_c/v = 0.82$, $v = 50$ cm^{-1}, and T = 300 K.

IV. AUGMENTING THE EQUILIBRIUM PROJECTOR WITH DYNAMICAL DERIVATIVES

Adding derivatives of the motion to the projector can offer an easy strategy to obtain an even swifter evaluation of the transport coefficient, i.e., a faster-decaying memory kernel. Here we augment our Mori projector of Eq. S8 with the time derivative of the current,

$$\begin{aligned}\hat{\zeta} &\equiv i[\hat{H}, \hat{J}] \\ &= d \sum_{\langle mn \rangle} v_{mn}(\hat{a}_m^\dagger \hat{a}_n + \hat{a}_n^\dagger \hat{a}_m)\Big(\epsilon_m - \epsilon_n + \sum_\alpha c_{m,\alpha}\hat{X}_{m,\alpha} - c_{n,\alpha}\hat{X}_{n,\alpha}\Big),\end{aligned} \tag{S15}$$

which includes the coordinates of the nuclear modes $\hat{X}_{i,\alpha}$.

Since HEOM integrates over the bosonic environment, one cannot *directly* measure ζ. However, one can employ finite difference on C_{JJ} to obtain a numerical approximation to $\dot{C}_{JJ}(t) = C_{J\zeta}(t) = -C_{\zeta J}(t)$, and, upon applying the finite difference derivative a second time, $\ddot{C}_{JJ}(t) = -C_{\zeta\zeta}(t)$. To confirm that this approximation is sufficiently accurate, we employ HEOM to calculate the polarization autocorrelation function, $C_{PP}(t)$, and compare its numerical time derivatives with the direct HEOM calculation of $C_{PJ}(t)$, $C_{JP}(t)$ and $C_{JJ}(t)$. We employ a linear (open-chain) topology for the Holstein model for this test as it circumvents the ambiguity in the definition of polarization in a periodic topology. As Fig. S2 shows, we obtain numerical agreement between $-\ddot{C}_{PP}(t)$ and $C_{JJ}(t)$. Hence, the time resolution in our HEOM simulations enables us to use numerical time derivatives to augment the projector numerically.

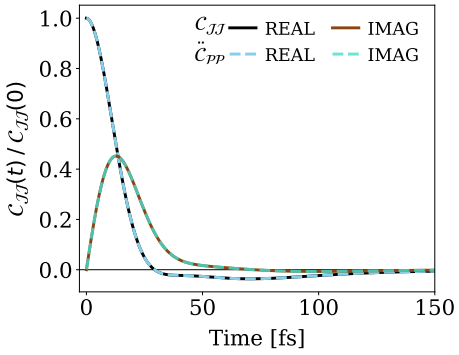

FIG. S2. The agreement of real and imaginary parts between the negative of the numerical double derivative of $C_{PP}(t)$ i.e. $-\ddot{C}_{PP}(t)$ and $C_{JJ}(t)$ in the linear topology for $\eta/v = 6.46, \omega_c/v = 0.81$, $v = 50$ cm^{-1}, and T = 300 K.

Augmenting the projection with the derivatives of the current results, naively, in the following 2×2 matrix,

$$\tilde{\mathcal{C}}(t) = \begin{pmatrix} C_{JJ}(t) & C_{J\zeta}(t) \\ C_{\zeta J}(t) & C_{\zeta\zeta}(t) \end{pmatrix}. \tag{S16}$$

However, $\tilde{\mathcal{C}}(t=0) \neq \mathbb{1}$, indicating that the projector is not idempotent. To fix this problem, we multiply the dynamical matrix by its inverse at $t = 0$,

$$\mathcal{C}(t) = \tilde{\mathcal{C}}(t)\tilde{\mathcal{C}}(0)^{-1}, \tag{S17}$$

ensuring $\mathcal{C}(t=0) = \mathbb{1}$. We can then use Eq. S9 to compute the memory kernel. As we show in the main text, augmenting the projector with derivatives of the original dynamical variable can shorten the memory kernel lifetime and result in significant computational savings.

V. CURRENT AND MEMORY KERNEL FITTING

The widely invoked Drude-Smith model offers a two-parameter analytical approximation for the current autocorrelation function and interprets conductance measurements. The MNZ approach to the current autocorrelation function offers an exact means to obtain its memory kernel. Hence, we employ our Mori GQME to assess the validity of the Drude-Smith approach.

In Laplace space, Eq. S9 takes the form,[S16]

$$C_{JJ}^{\mathrm{Kubo}}(\omega) = \frac{1}{\mathcal{K}^{\mathrm{Kubo}}(\omega) + \mathrm{i}\omega}. \tag{S18}$$

Ref S17 has shown that the Drude-Smith form can arise from setting the memory kernel to $\mathcal{K}^{\mathrm{Kubo}}(t) = q\exp(-rt)$, moving to Laplace space, solving for the roots that lead to a singularity in Eq. S18, and considering *only* the case where the two poles are degenerate, i.e., $r = 2\sqrt{q}$. A general solution would consider two distinct, complex poles $2\omega_{\pm} = r \pm \sqrt{r^2 - 4q}$ which give two different decay terms after an inverse Laplace transform,

$$C_{JJ}^{\mathrm{Kubo}}(t)/C_{JJ}^{\mathrm{Kubo}}(0) = \frac{(\omega_+ - r)\mathrm{e}^{-\omega_+ t} + (r - \omega_-)\mathrm{e}^{-\omega_- t}}{(\omega_+ - \omega_-)}. \tag{S19}$$

This motivates employing a more flexible form to fit our exact current autocorrelation functions,

$$C_{JJ}^{\mathrm{Kubo}}(t)/C_{JJ}^{\mathrm{Kubo}}(0) = \sum_{i}^{n_{\mathrm{fit}}} a_i \cos(\omega_i t)\mathrm{e}^{-k_i t}. \tag{S20}$$

With 5 parameters ($n_{\mathrm{fit}} = 2$ and $a_1 + a_2 = 1$ is a constraint) we are guaranteed to obtain a better fit, but one can observe from Fig. S3 that the oscillatory frequencies are qualitatively wrong. By extension, Eq. S19 cannot fit the data. We must conclude that $\mathcal{K}^{\mathrm{Kubo}}(t)$ is not well-described by a single exponential. Further, a single exponential in time would yield a Lorentzian in frequency, but our simplest $\tilde{\mathcal{K}}(\omega)$ is instead a Gaussian. Indeed, using just decaying exponentials in time, $\mathcal{K}^{\mathrm{Kubo}}(t) = \sum_i \alpha_i \exp(-\kappa_i t)$, we find that using even five terms is insufficient to describe the data of Fig. 4.

We fit the $C_{JJ}^{\mathrm{Kubo}}(t)$ using Eq. S20 for 16 points in the parameter space with $n_{\mathrm{fit}} = 2$. The fits are closer than the Drude-Smith form, but are clearly qualitatively lacking. Figure S3 shows an example where $[\eta/v, \omega_c/v] = [100/50, 25/50]$. Table. I summarizes the corresponding fit parameters. Unlike the Drude-Smith form, neither term has a negative coefficient. Our analysis of this Drude-Smith fitting protocol suggests that decomposing the current autocorrelation function reporting on small polaron transport into decaying and oscillatory exponentials can lead to significant ambiguities, motivating our cumulant-based analysis in the main text.

i^{th} term	a_i	ω_i [fs^{-1}]	k_i [fs^{-1}]
1	0.7386	0.0169	0.0143
2	0.2614	0.0359	0.0147

TABLE I. Fit parameters for $C_{JJ}^{\mathrm{Kubo}}(t)$ in Fig. S3 for $\eta/v = 2, \omega_c/v = 0.5$, $v = 50$ cm^{-1}, and T = 300 K.

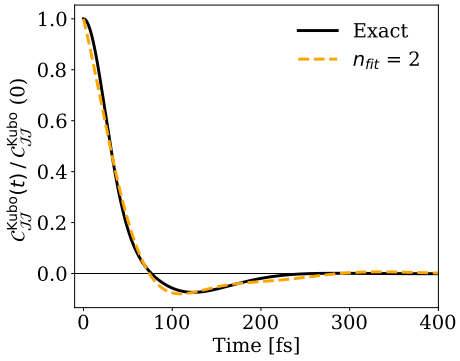

FIG. S3. Two damped cosine fit (orange) according to Eq. S20 to the C_{JJ}^{Kubo} obtained with HEOM (black) for $\eta/v = 2, \omega_c/v = 0.5$, $v = 50$ cm^{-1}, and T = 300 K. The 5-parameters fit is not sufficient to capture the C_{JJ}^{Kubo}.

VI. CUMULANT-BASED ANALYSIS

We now provide a detailed description of our backmapping technique. It employs the normalized real part of the Kubo memory kernel in frequency space, $\tilde{\mathcal{K}}(\omega)$, which one obtains from $\mathcal{K}^{\mathrm{Kubo}}(\omega)$ as mentioned in the main text,

$$\tilde{\mathcal{K}}(\omega) = \mathbb{Re}\left[\mathcal{K}^{\mathrm{Kubo}}(\omega)\right] / \mathbb{Re}\left[\int \mathrm{d}\omega\, \mathcal{K}^{\mathrm{Kubo}}(\omega)\right]. \tag{S21}$$

Below, we show theoretical ways of extracting $\tilde{\mathcal{K}}(\omega)$ and then demonstrate how to extract the same quantity from experimentally accessible data. Specifically, one can compute $\mathcal{K}^{\mathrm{Kubo}}(\omega)$ in two ways: 1) from the Fourier-Laplace transform of the time-domain Kubo memory kernel $\mathcal{K}^{\mathrm{Kubo}}(t)$, which can be accessed through the GQME Eq. S9; or from Eq. S18 where we employ the frequency-domain correlation function $C_{JJ}^{\mathrm{Kubo}}(\omega)$. Both approaches require the normalized time-domain correlation function, $C_{JJ}^{\mathrm{Kubo}}(t)$. While this correlation function must, in general, be computed using one's choice of dynamical method (e.g., HEOM), we show that one can extract $\tilde{\mathcal{K}}(\omega)$ using only the experimentally accessible $\sigma(\omega)$. In particular, one can show that:

$$\tilde{\mathcal{K}}(\omega) = \mathbb{Re}\left[1/\sigma(\omega)\right] / \mathbb{Re}\left[\int \mathrm{d}\omega\, 1/\sigma(\omega)\right]. \tag{S22}$$

Thus, when an experiment gives access to $\sigma(\omega)$, one can directly follow our backmapping strategy to infer the appropriate parameter regime of the dispersive Holstein Hamiltonian using $\tilde{\mathcal{K}}(\omega)$, as we showed with our theoretical data in the main text. We note that one should be able to generalize this procedure to other models that users may find more relevant for their particular applications.

VII. CURRENT AUTOCORRELATION FUNCTIONS AND CONDUCTIVITY RESPONSES FOR THE DISPERSIVE HOLSTEIN MODEL

Here, we display the current autocorrelation functions and conductivity for the homogeneous, 1-dimensional dispersive Holstein model in the thermodynamic limit as one varies the charge-lattice coupling, η, and characteristic frequency of the local lattice phonons, ω_c, for $v = 50$ cm^{-1} and T = 300 K.

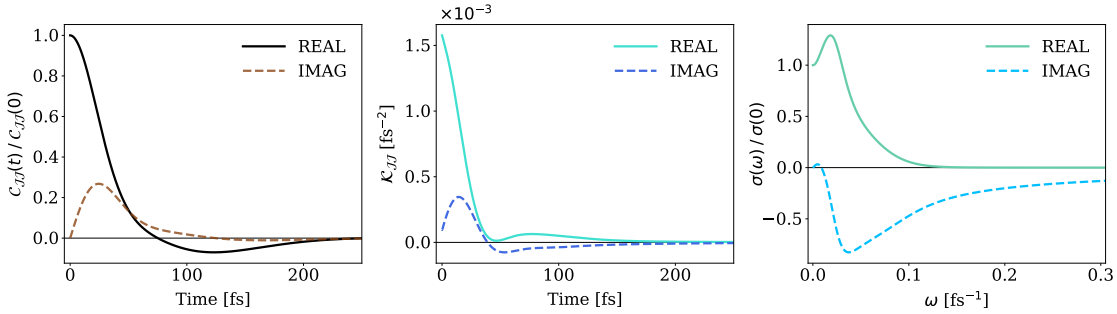

FIG. S4. Parameters: $\eta/v = 2.0$, $\omega_c/v = 0.5$. **Left**: Current autocorrelation function, $C_{JJ}(t)$. **Middle**: Memory kernel, $\mathcal{K}(t)$ with lifetime $\tau_K = 317$ fs. **Right**: Real and imaginary part of the conductance, $\sigma(\omega)$.

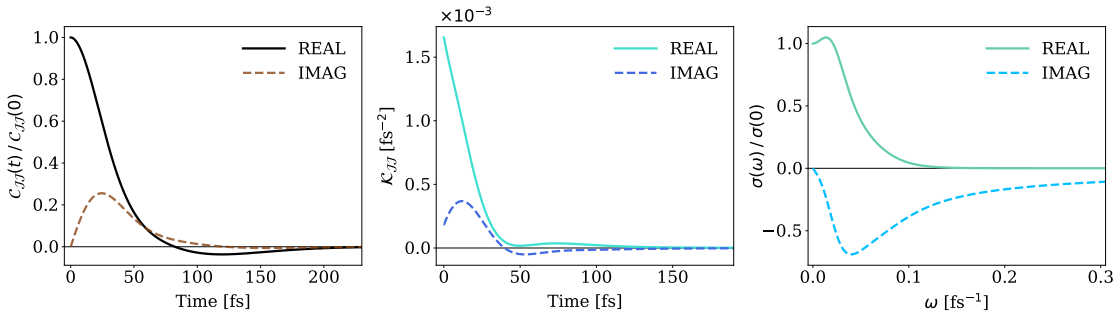

FIG. S5. Parameters: $\eta/v = 2.0$, $\omega_c/v = 1.0$. **Left**: Current autocorrelation function, $C_{JJ}(t)$. **Middle**: Memory kernel, $\mathcal{K}(t)$ with lifetime $\tau_K = 164$ fs. **Right**: Real and imaginary part of the conductance, $\sigma(\omega)$.

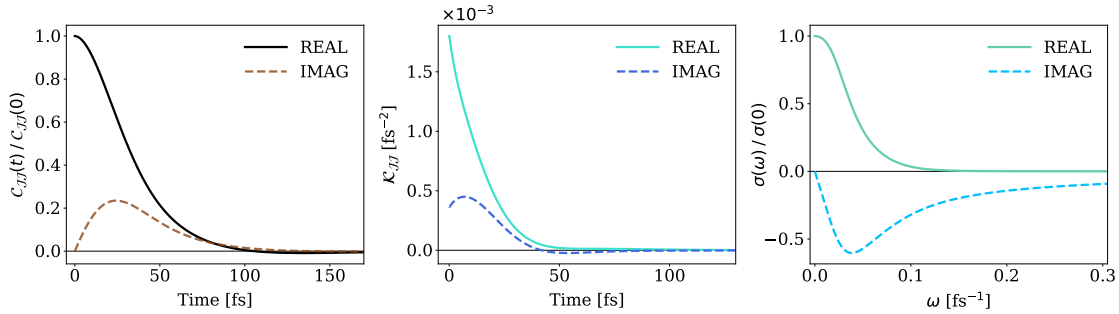

FIG. S6. Parameters: $\eta/v = 2.0$, $\omega_c/v = 2.0$. **Left**: Current autocorrelation function, $C_{JJ}(t)$. **Middle**: Memory kernel, $\mathcal{K}(t)$ with lifetime $\tau_K = 167$ fs. **Right**: Real and imaginary part of the conductance, $\sigma(\omega)$.

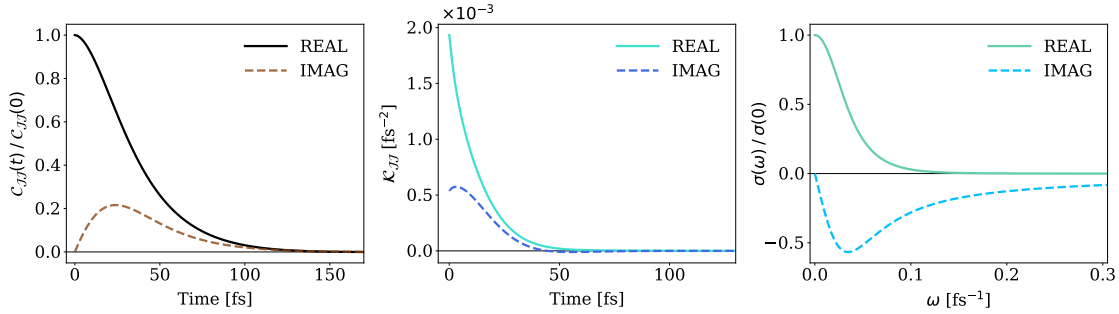

FIG. S7. Parameters: $\eta/v = 2.0$, $\omega_c/v = 3.0$. **Left**: Current autocorrelation function, $C_{JJ}(t)$. **Middle**: Memory kernel, $\mathcal{K}(t)$ with lifetime $\tau_K = 65$ fs. **Right**: Real and imaginary part of the conductance, $\sigma(\omega)$.

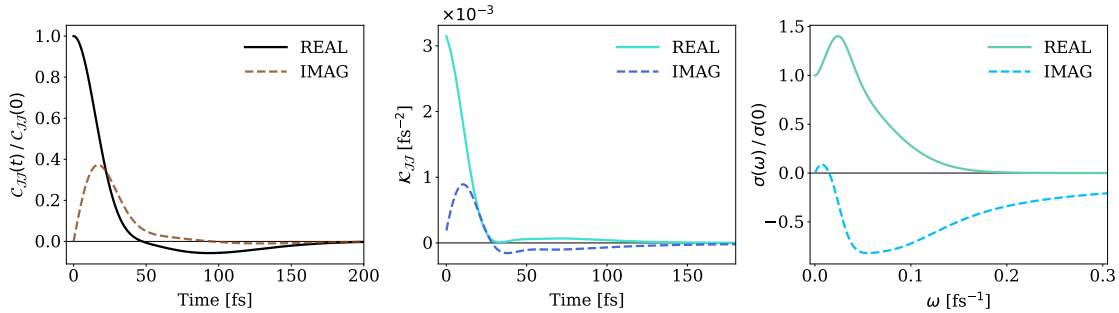

FIG. S8. Parameters: $\eta/v = 4.0$, $\omega_c/v = 0.5$. **Left**: Current autocorrelation function, $C_{JJ}(t)$. **Middle**: Memory kernel, $\mathcal{K}(t)$ with lifetime $\tau_K = 337$ fs. **Right**: Real and imaginary part of the conductance, $\sigma(\omega)$.

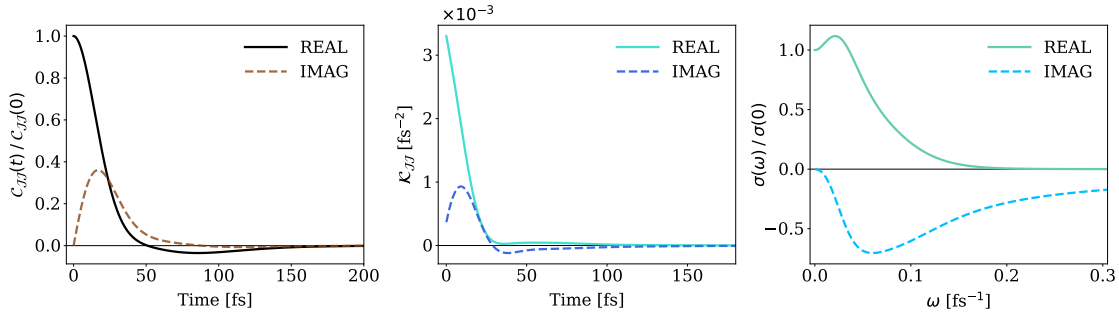

FIG. S9. Parameters: $\eta/v = 4.0$, $\omega_c/v = 1.0$. **Left**: Current autocorrelation function, $C_{JJ}(t)$. **Middle**: Memory kernel, $\mathcal{K}(t)$ with lifetime $\tau_K = 178$ fs. **Right**: Real and imaginary part of the conductance, $\sigma(\omega)$.

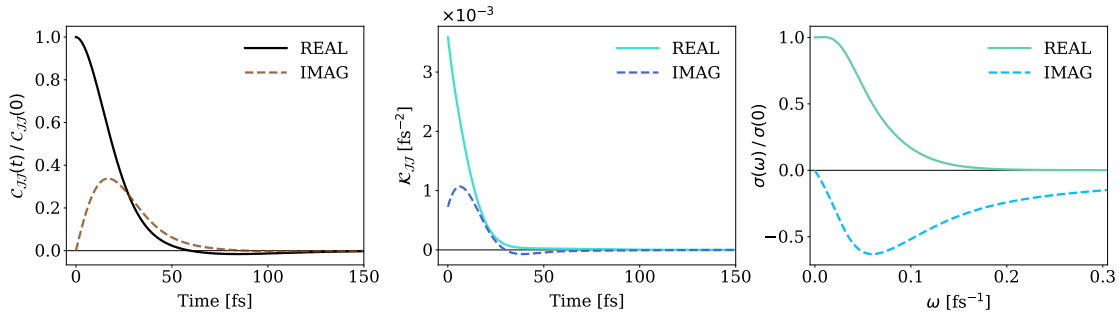

FIG. S10. Parameters: $\eta/v = 4.0$, $\omega_c/v = 2.0$. **Left**: Current autocorrelation function, $C_{JJ}(t)$. **Middle**: Memory kernel, $\mathcal{K}(t)$ with lifetime $\tau_K = 93$ fs. **Right**: Real and imaginary part of the conductance, $\sigma(\omega)$.

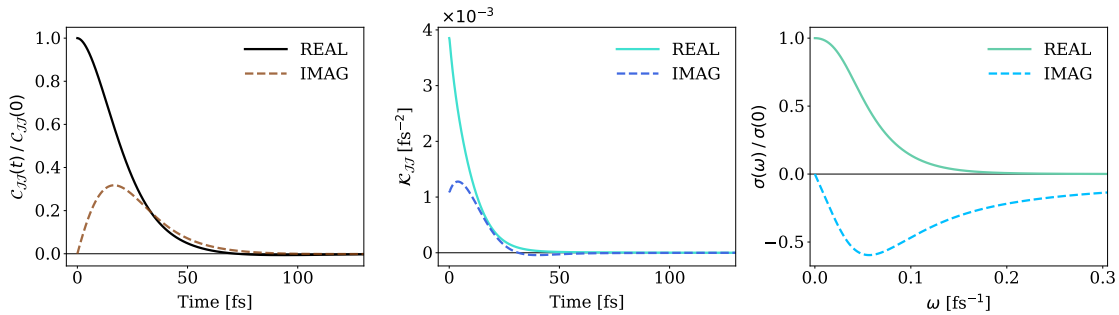

FIG. S11. Parameters: $\eta/v = 4.0$, $\omega_c/v = 3.0$. **Left**: Current autocorrelation function, $C_{JJ}(t)$. **Middle**: Memory kernel, $\mathcal{K}(t)$ with lifetime $\tau_K = 60$ fs. **Right**: Real and imaginary part of the conductance, $\sigma(\omega)$.

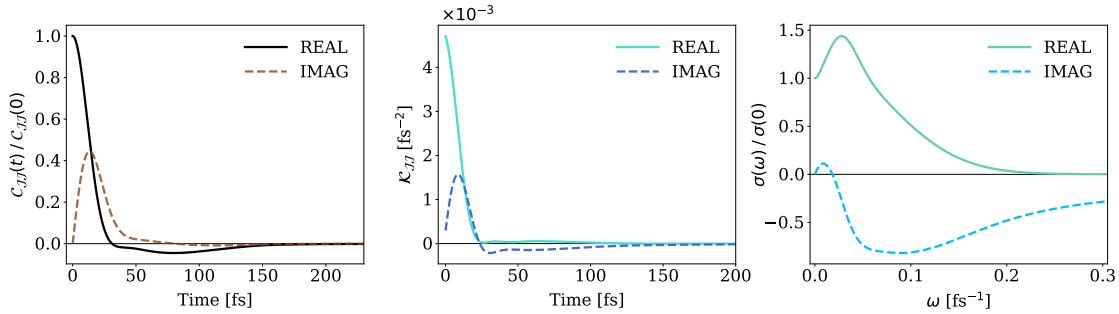

FIG. S12. Parameters: $\eta/v = 6.0$, $\omega_c/v = 0.5$. **Left**: Current autocorrelation function, $C_{JJ}(t)$. **Middle**: Memory kernel, $\mathcal{K}(t)$ with lifetime $\tau_K = 305$ fs. **Right**: Real and imaginary part of the conductance, $\sigma(\omega)$.

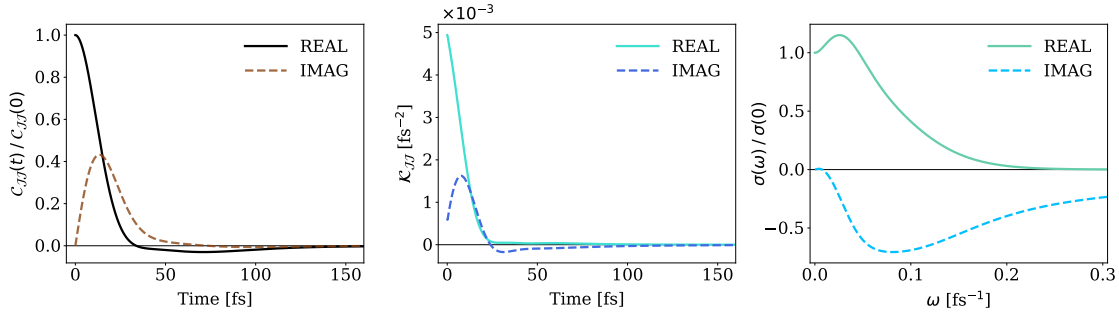

FIG. S13. Parameters: $\eta/v = 6.0$, $\omega_c/v = 1.0$. **Left**: Current autocorrelation function, $C_{JJ}(t)$. **Middle**: Memory kernel, $\mathcal{K}(t)$ with lifetime $\tau_K = 189$ fs. **Right**: Real and imaginary part of the conductance, $\sigma(\omega)$.

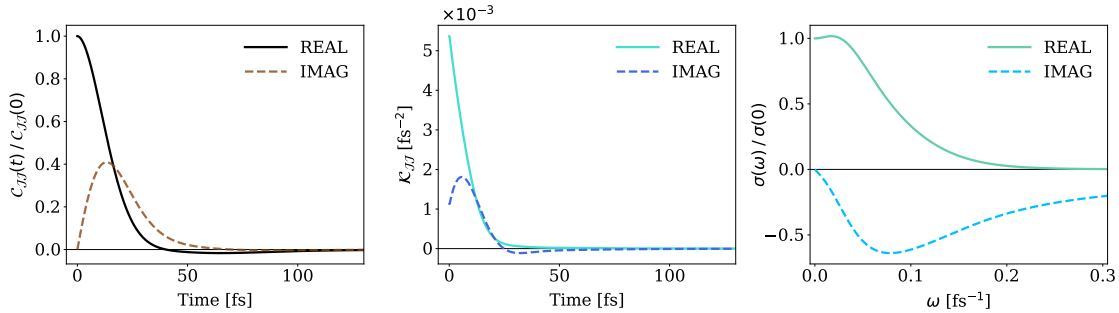

FIG. S14. Parameters: $\eta/v = 6.0$, $\omega_c/v = 2.0$. **Left**: Current autocorrelation function, $C_{JJ}(t)$. **Middle**: Memory kernel, $\mathcal{K}(t)$ with lifetime $\tau_K = 96$ fs. **Right**: Real and imaginary part of the conductance, $\sigma(\omega)$.

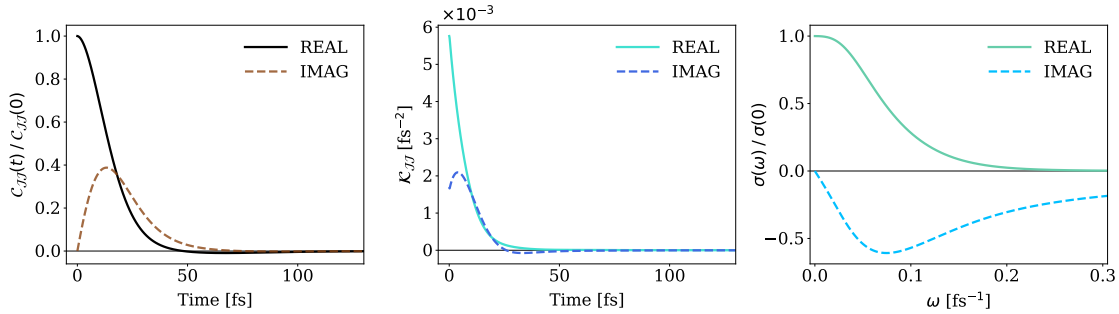

FIG. S15. Parameters: $\eta/v = 6.0$, $\omega_c/v = 3.0$. **Left**: Current autocorrelation function, $C_{JJ}(t)$. **Middle**: Memory kernel, $\mathcal{K}(t)$ with lifetime $\tau_K = 61$ fs. **Right**: Real and imaginary part of the conductance, $\sigma(\omega)$.

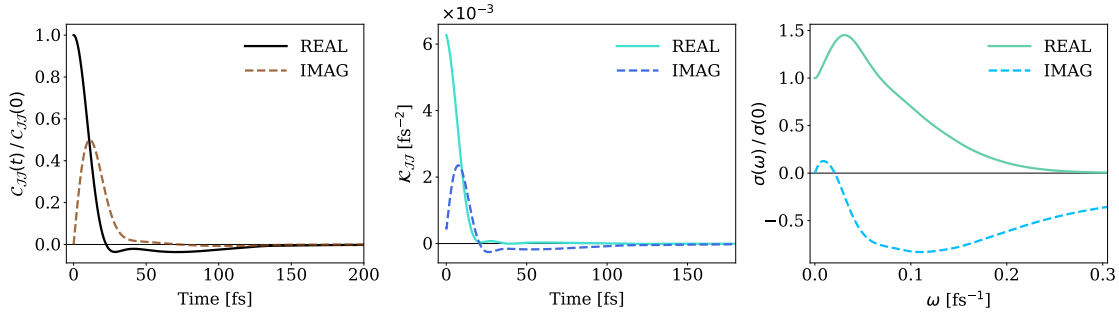

FIG. S16. Parameters: $\eta/v = 8.0$, $\omega_c/v = 0.5$. **Left**: Current autocorrelation function, $C_{JJ}(t)$. **Middle**: Memory kernel, $\mathcal{K}(t)$ with lifetime $\tau_K = 378$ fs. **Right**: Real and imaginary part of the conductance, $\sigma(\omega)$.

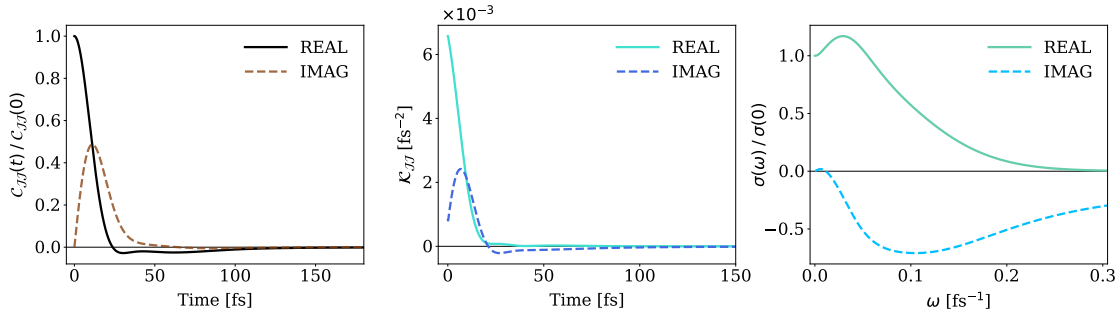

FIG. S17. Parameters: $\eta/v = 8.0$, $\omega_c/v = 1.0$. **Left**: Current autocorrelation function, $C_{JJ}(t)$. **Middle**: Memory kernel, $\mathcal{K}(t)$ with lifetime $\tau_K = 195$ fs. **Right**: Real and imaginary part of the conductance, $\sigma(\omega)$.

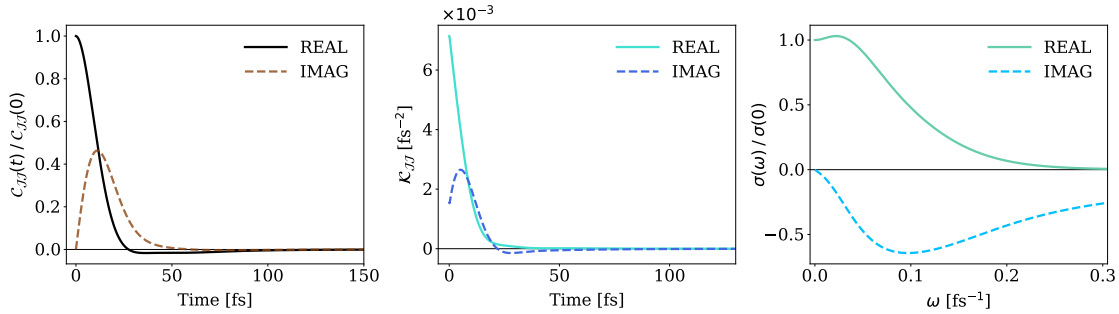

FIG. S18. Parameters: $\eta/v = 8.0$, $\omega_c/v = 2.0$. **Left**: Current autocorrelation function, $C_{JJ}(t)$. **Middle**: Memory kernel, $\mathcal{K}(t)$ with lifetime $\tau_K = 96$ fs. **Right**: Real and imaginary part of the conductance, $\sigma(\omega)$.

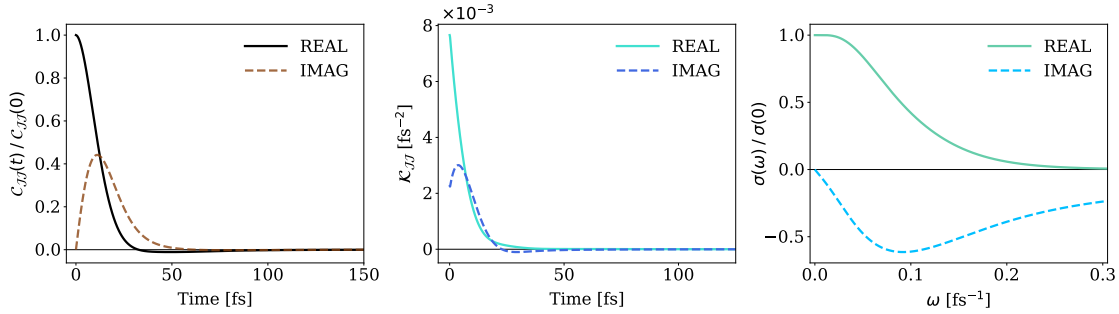

FIG. S19. Parameters: $\eta/v = 8.0$, $\omega_c/v = 3.0$. **Left**: Current autocorrelation function, $C_{JJ}(t)$. **Middle**: Memory kernel, $\mathcal{K}(t)$ with lifetime $\tau_K = 62$ fs. **Right**: Real and imaginary part of the conductance, $\sigma(\omega)$.

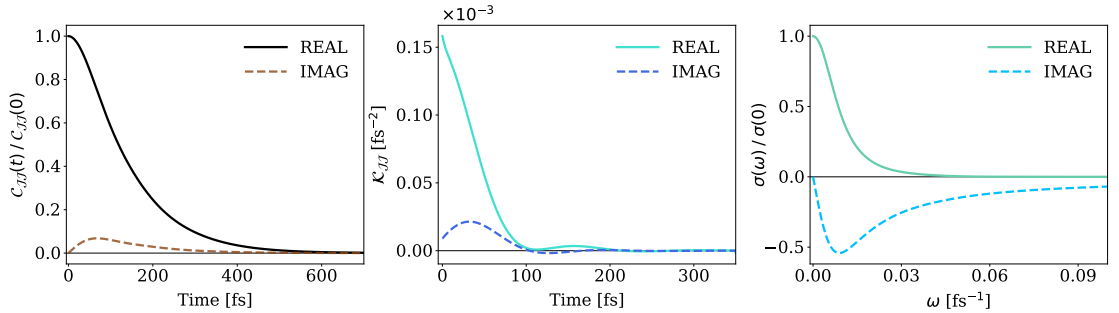

FIG. S20. Parameters: $\eta/v = 0.2$, $\omega_c/v = 0.5$. **Left**: Current autocorrelation function, $C_{JJ}(t)$. **Middle**: Memory kernel, $\mathcal{K}(t)$ with lifetime $\tau_K = 173$ fs. **Right**: Real and imaginary part of the conductance, $\sigma(\omega)$.

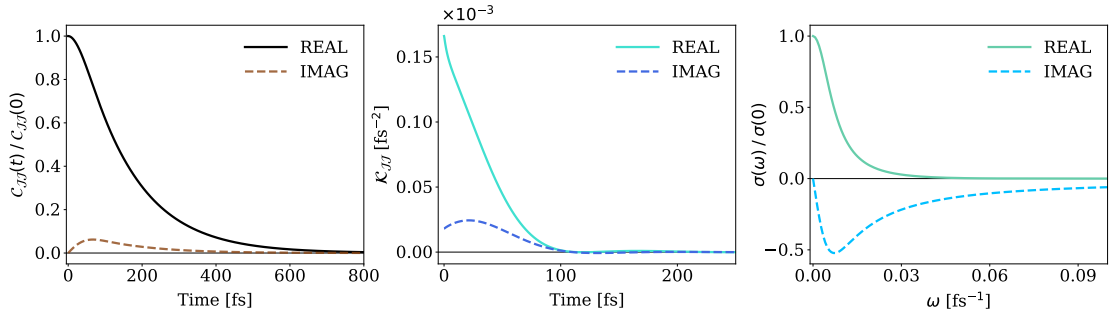

FIG. S21. Parameters: $\eta/v = 0.2$, $\omega_c/v = 1.0$. **Left**: Current autocorrelation function, $C_{JJ}(t)$. **Middle**: Memory kernel, $\mathcal{K}(t)$ with lifetime $\tau_K = 105$ fs. **Right**: Real and imaginary part of the conductance, $\sigma(\omega)$.

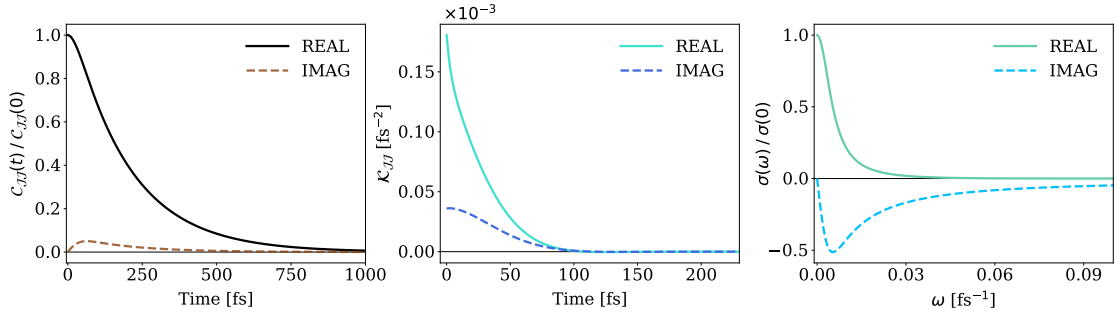

FIG. S22. Parameters: $\eta/v = 0.2$, $\omega_c/v = 2.0$. **Left**: Current autocorrelation function, $C_{JJ}(t)$. **Middle**: Memory kernel, $\mathcal{K}(t)$ with lifetime $\tau_K = 80$ fs. **Right**: Real and imaginary part of the conductance, $\sigma(\omega)$.

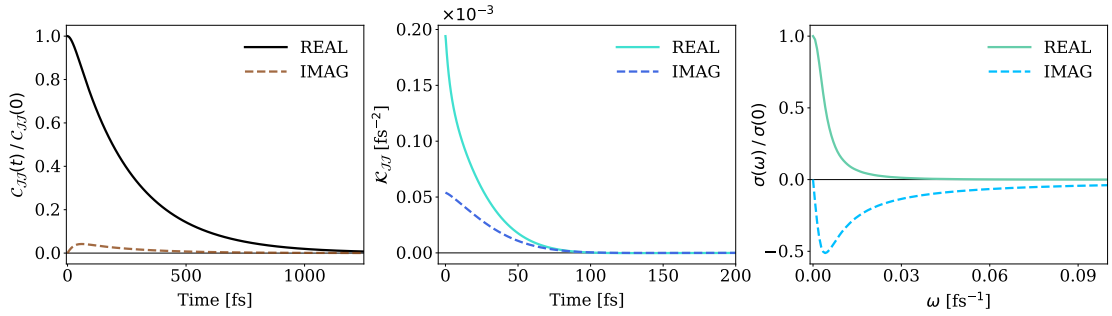

FIG. S23. Parameters: $\eta/v = 0.2$, $\omega_c/v = 3.0$. **Left**: Current autocorrelation function, $C_{JJ}(t)$. **Middle**: Memory kernel, $\mathcal{K}(t)$ with lifetime $\tau_K = 74$ fs. **Right**: Real and imaginary part of the conductance, $\sigma(\omega)$.

REFERENCES

[S1]S. Bhattacharyya, T. Sayer, and A. Montoya-Castillo, "Anomalous transport of small polarons arises from transient lattice relaxation or immovable boundaries," Journal of Physical Chemistry Letters **15**, 1382–1389 (2024).

[S2]J. Bosse and Y. Kaneko, "Self-diffusion in supercooled binary liquids," Physical Review Letters **74**, 4023 (1995).

[S3]D. R. Reichman and E. Rabani, "Self-consistent mode-coupling theory for self-diffusion in quantum liquids," Physical Review Letters **87**, 265702 (2001).

[S4]D. R. Reichman and E. Rabani, "A self-consistent mode-coupling theory for dynamical correlations in quantum liquids: Application to liquid para-hydrogen," Journal of Chemical Physics **116**, 6279–6285 (2002).

[S5]A. Montoya-Castillo and D. R. Reichman, "Approximate but accurate quantum dynamics from the mori formalism: I. nonequilibrium dynamics," Journal of Chemical Physics **144**, 184104 (2016).

[S6]A. Kelly, A. Montoya-Castillo, L. Wang, and T. E. Markland, "Generalized quantum master equations in and out of equilibrium: When can one win?" Journal of Chemical Physics **144**, 184105 (2016).

[S7]A. Montoya-Castillo and D. R. Reichman, "Approximate but accurate quantum dynamics from the mori formalism. ii. equilibrium time correlation functions," Journal of Chemical Physics **146**, 084110 (2017).

[S8]Q. Shi and E. Geva, "A new approach to calculating the memory kernel of the generalized quantum master equation for an arbitrary system–bath coupling," Journal of Chemical Physics **119**, 12063–12076 (2003).

[S9]M.-L. Zhang, B. J. Ka, and E. Geva, "Nonequilibrium quantum dynamics in the condensed phase via the generalized quantum master equation," Journal of Chemical Physics **125**, 044106 (2006).

[S10]W. C. Pfalzgraff, A. Montoya-Castillo, A. Kelly, and T. E. Markland, "Efficient construction of generalized master equation memory kernels for multi-state systems from nonadiabatic quantum-classical dynamics," Journal of Chemical Physics **150**, 244109 (2019).

[S11]E. Süli and D. F. Mayers, *An introduction to numerical analysis* (Cambridge university press, 2003).

[S12]M. Sparpaglione and S. Mukamel, "Dielectric friction and the transition from adiabatic to nonadiabatic electron transfer. i. solvation dynamics in liouville space," Journal of Chemical Physics **88**, 3263–3280 (1988).

[S13]A. A. Golosov and D. R. Reichman, "Reference system master equation approaches to condensed phase charge transfer processes. i. general formulation," Journal of Chemical Physics **115**, 9848–9861 (2001).

[S14]Y. Yan, M. Xu, Y. Liu, and Q. Shi, "Theoretical study of charge carrier transport in organic molecular crystals using the nakajima-zwanzig-mori generalized master equation," Journal of Chemical Physics **150**, 234101 (2019).

[S15]L. Song and Q. Shi, "A new approach to calculate charge carrier transport mobility in organic molecular crystals from imaginary time path integral simulations," Journal of Chemical Physics **142**, 174103 (2015).

[S16]D. Forster, *Hydrodynamic fluctuations, broken symmetry, and correlation functions* (CRC Press, 2018).

[S17]W.-C. Chen and R. A. Marcus, "The drude-smith equation and related equations for the frequency-dependent electrical conductivity of materials: Insight from a memory function formalism," ChemPhysChem **22**, 1667–1674 (2021).